Journal of Advanced Ceramics
2022, **11**(3): 515–521
https://doi.org/10.1007/s40145-021-0548-0
ISSN 2226-4108
CN 10-1154/TQ

Rapid Communication

Modulation of spin dynamics in Ni/Pb($Mg_{1/3}Nb_{2/3}$)O_3–$PbTiO_3$ multiferroic heterostructure

Hang XU[a,b], Bo WANG[a], Ji QI[a,b], Mei LIU[a], Fei TENG[a,c,*], Linglong HU[a], Yuan ZHANG[a], Chaoqun QU[a,*], Ming FENG[a,*]

[a]*Key Laboratory of Functional Materials Physics and Chemistry of the Ministry of Education, Jilin Normal University, Changchun 130103, China*
[b]*Condensed Matter Science and Technology Institute, School of Instrumentation Science and Engineering, Harbin Institute of Technology, Harbin 150080, China*
[c]*College of Mathematics, Jilin Normal University, Siping 136000, China*

Received: July 8, 2021; Revised: Octorber 4, 2021; Accepted: Octorber 16, 2021

Abstract: Motivated by the fast-developing spin dynamics in ferromagnetic/piezoelectric structures, this study attempts to manipulate magnons (spin-wave excitations) by the converse magnetoelectric (ME) coupling. Herein, electric field (*E*-field) tuning magnetism, especially the surface spin wave, is accomplished in Ni/0.7Pb($Mg_{1/3}Nb_{2/3}$)O_3–0.3$PbTiO_3$ (PMN–PT) multiferroic heterostructures. The Kerr signal (directly proportional to magnetization) changes of Ni film are observed when direct current (DC) or alternative current (AC) voltage is applied to PMN–PT substrate, where the signal can be modulated breezily even without extra magnetic field (*H*-field) in AC-mode measurement. Deserved to be mentioned, a surface spin wave switch of "1" (i.e., "on") and "0" (i.e., "off") has been created at room temperature upon applying an *E*-field. In addition, the magnetic anisotropy of heterostructures has been investigated by *E*-field-induced ferromagnetic resonance (FMR) shift, and a large 490 Oe shift of FMR is determined at the angle of 45° between *H*-field and heterostructure plane.

Keywords: spin dynamics; multiferroic heterostructure; non-volatile; magnetic anisotropy; spin wave switch

1 Introduction

Multiferroic heterostructures constricted from ferroelectric (FE) and ferromagnetic (FM) phases are widely applied in new functionalities and devices, such as microwave devices, sensors, logic circuits, nonvolatile memory, and spintronics devices [1–7]. In recent years, with the ever-increasing demand for fast, small, energy-efficient, and non-volatile electronic devices, the investigation of electric field (*E*-field) manipulating spin degree of freedom and magnetic states has launched a blast of the upsurge in FM/FE heterostructures [8–13]. Compared with conventional current trigger and magnetic field (*H*-field) tuned devices, these *E*-field-manipulatable multiferroic devices exhibit ultra-low power consumption, fast computing, better compactness, and light weight

* Corresponding authors.
E-mail: F. Teng, tengf666@jlnu.edu.cn;
C. Qu, quchaoqun@jlnu.edu.cn;
M. Feng, mingfeng@jlnu.edu.cn

[14–17]. Artificial FM/FE multiferroic heterostructures are of great potential for devices due to their strong magnetoelectric (ME) coupling, that is, *E*-field regulates magnetism or *vice versa*. Various characteristics related to magnetics have been dominated by *E*-field in the multiferroic system, such as Curie temperature (T_C) [18–20], magnetic domain [20–22], magnetoresistance [23–25], and ferromagnetic resonance (FMR) [16,26].

As we all know, the ME coupling effects include strain/stress, interfacial charge, and exchange bias in FM/FE multiferroic heterostructures [27,28]. Clearing the competition and coexistence of those mechanisms also presents an arresting diversity in metal and metallic oxide. As a typical magnetoresistive material, Ni is usually chosen to be used as the FM phase since it is a prototype of 3D itinerant ferromagnet with a high Curie temperature (T_C = 631 K) [29]. Moreover, Ni is also an ideal material for extensive applications in sensors due to its high-temperature stability, anti-corrosion, and abrasive resistance [30–34]. $0.7Pb(Mg_{1/3}Nb_{2/3})O_3$–$0.3PbTiO_3$ (PMN–PT) single crystal is a well-known piezoelectric material, which is desired for FM/FE heterostructures because of its giant anisotropic piezoelectric coefficients and low loss tangents [35–39].

Different from the correlated transition metal oxides such as $La_{2/3}Sr_{1/3}MnO_3$ and Fe_3O_4, whose electron–phonon interaction is strong enough to obtain a substantial strain-modulable electronic/magnetic structure, pure 3D metal Ni with a higher carrier density is conventionally treated as a kind of stubborn materials leaking efficient approaches for tunability [27,32,40]. Nonetheless, to achieve the information of possible spin dynamic response, which may benefit the further spintronics devices and new energy applications, we focus on the multiferroic heterostructure composed of Ni and PMN–PT to seek a comprehensive understanding of the characteristic of 3D metal as a function of strain. In 2017, Zhu *et al*. [41] explored the excitation of surface spin wave in $La_{0.7}Sr_{0.3}MnO_3$ (LSMO)/PMN–PT based on strain/stress at 193 K. Enlightened by the accomplishment of the above, we are devoted to studying *E*-field which dominates the surface spin wave at room temperature in Ni/PMN–PT. In this study, it was observed that the application of voltage not only causes an FMR shift but also excites the surface spin wave at room temperature. The tunable multiferroic heterostructures represent great opportunities for new electronic devices.

2 Experimental

In this experiment, the Ni/PMN–PT multiferroic heterostructures were fabricated by direct sedimentation of Ni films onto the commercial and polished (011)-oriented PMN–PT using a magnetron sputtering (MS) method. The pure Ni target with a diameter of 50.8 mm was used, and the argon was used as the sputtering gas. At first, the vacuum of the main chamber reached 7×10^{-7} Torr before growing Ni film. Then the temperature of PMN–PT was maintained at 200 ℃, and the sputtering power was 80 W with the constant argon pressure of 4×10^{-2} Torr during deposition. Finally, the Ni/PMN–PT samples were annealed to room temperature.

The surface and cross-sectional morphologies of the Ni/PMN–PT heterostructures were characterized by atomic force microscope (AFM; Asylum Research, MFP-3D, UK) and focused ion beam scanning electron microscope (FIB-SEM; Thermo Scientific, Scios 2, USA), respectively. The Kerr hysteresis loops were determined by magneto-optical Kerr effect (MOKE; Durham Magneto Optics Ltd., Nano MOKE^{TM} 3, UK) magnetometer, and the FMR was performed with an electron spin resonance (ESR; JEOL, JES-FA200, Japan) system. The direct current (DC) voltage was applied by a Keithley 2410 (USA), and the alternative current (AC) voltage was applied by a Keysight 6804A (USA).

3 Results and discussion

In this study, a reversible *E*-field tuning FMR shift in Ni/PMN–PT heterostructures was achieved by using the ESR device. The back of PMN–PT (5 mm × 4 mm × 0.3 mm) was coated by a thin layer of platinum as the base electrode, the Ni layer as the top electrode. Figure 1(a) shows the schematic diagram of *E*-field control ESR measurement in Ni/PMN–PT heterostructures at out-of-plane orientation, i.e., *H*-field perpendicular to the sample plane (90°), where in-plane orientation is *H*-field parallel to the sample plane (0°). The PMN–PT single crystal produced strain when a vertical applied *E*-field was across it, and the *P*–*E* loop and ε_{33}–*E* curve of PMN–PT are displayed in Fig. 1(b), which presents the PMN–PT with a coercive field of 2.6 kV/cm, and a remnant and saturation polarization of 52 and 62 μC/cm^2 under 10 kV/cm, respectively.

As shown in Fig. 2(a), the Ni film exhibits a smooth

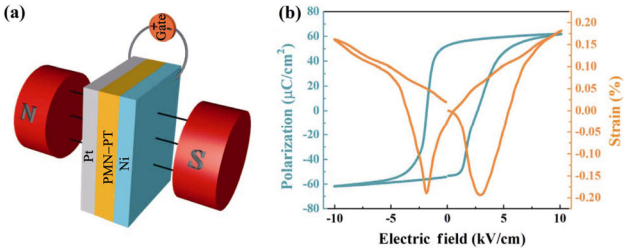

Fig. 1 (a) Schematic illustration of ESR measurement in the Ni/PMN–PT multiferroic heterostructure (out-of-plane). (b) Polarization and out-of-plane strain as a function of the *E*-field across the PMN–PT(011) single crystal.

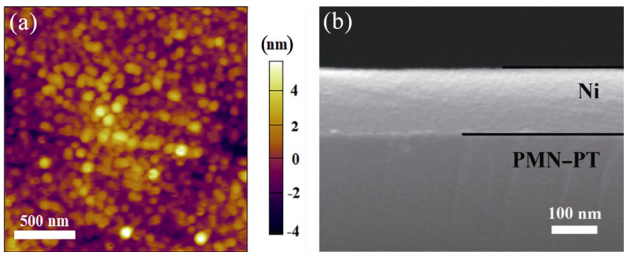

Fig. 2 (a) Surface and (b) cross-sectional morphology images of Ni thin film grown on PMN–PT.

and dense surface at the range of 2 μm × 2 μm. The cross-sectional morphology image presents that the thickness of Ni film is about 140 nm in Fig. 2(b).

Figure 3(a) shows the schematic diagram of MOKE measurement under varying applied voltages. A laser beam was focused on the surface of Ni film, and then DC or AC voltage would be applied to the PMN–PT substrate, where no external *H*-field was used in AC-mode measurement. Figures 3(b) and 3(c) display the in-plane Kerr hysteresis loops of Ni/PMN–PT under different *E*-fields when DC voltages were applied perpendicularly to the substrate. When the *E*-field increases to 6.7 and −6.7 kV/cm, it can be calculated that the coercive field will decrease by 10 and 20 Oe, respectively. Figure 3(d) presents a butterfly-shaped Kerr-*E* curve, which is similar to the ε_{33}–*E* loop of PMN–PT (Fig. 1(b)), providing specific evidence for stain-mediated converse ME coupling in Ni/PMN–PT. Under an *E*-field, the lattice constant of the PMN–PT substrate can be significantly changed due to its great piezoelectric property and *E*-field-induced strain in PMN–PT, and then delivered to Ni layer, leading to a deformation of the Ni film and attributing to the magnetoelastic effect. Because of the different piezoresponses of the PMN–PT under AC or DC voltage, the piezoresponse induced by AC is superior to the scenario of DC, which could be the intrinsic effect of our observation. In addition, although the electrodes were treated very carefully, the unperfect interface between electrode and PMN–PT may introduce space charges. Thus, under AC and DC voltages, these space charges may influence the effective *E*-field on PMN–PT as the defect effect.

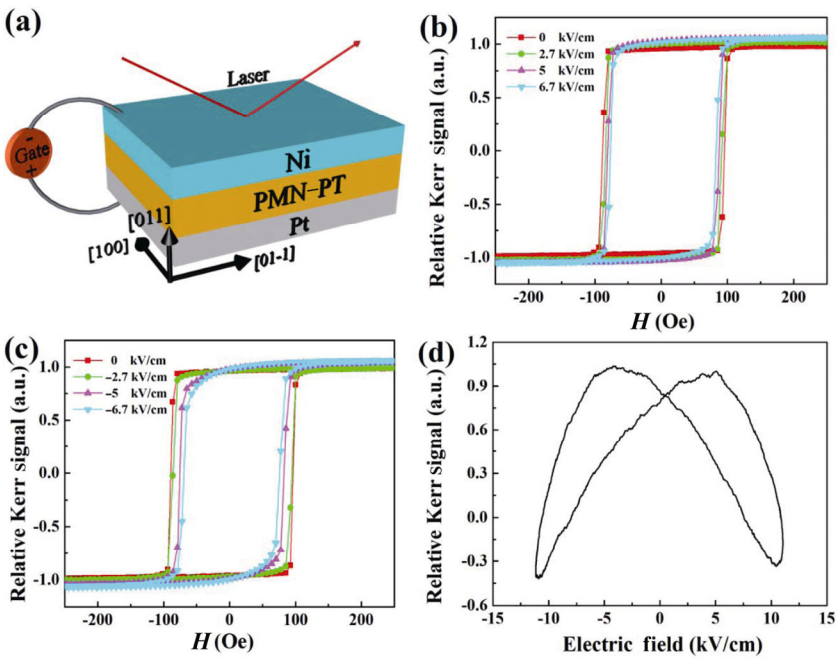

Fig. 3 (a) Schematic illustration of Ni/PMN–PT multiferroic heterostructure by MOKE measurement. In-plane Kerr hysteresis loops under positive (b) and negative (c) voltage. (d) *E*-field dependence of Kerr signal without external *H*-field in Ni/PMN–PT multiferroic heterostructure.

From the above results, it can be inferred that the magnetic anisotropy of the Ni/PMN–PT is due to the strain-mediated converse ME coupling. To prove it, the voltage-regulated ESR tests are compared to theoretical calculation values. The *E*-field-induced effective *H*-fields (H_{eff}) along different orientations are expressed as

$$H_{\text{eff},[01\bar{1}]}=\frac{3\lambda Y}{M_{\text{s}}(1+\nu)}(d_{31}-d_{32})E \quad (1)$$

$$H_{\text{eff},[100]}=\frac{-3\lambda Y}{M_{\text{s}}(1+\nu)}(d_{31}-d_{32})E \quad (2)$$

$$H_{\text{eff},[011]}=\frac{-3\lambda Y}{M_{\text{s}}(1+\nu)}(d_{31}+d_{32})E \quad (3)$$

where M_{s} is the saturation magnetization, d_{31} and d_{32} are the piezoelectric coefficients, Y is Young's modulus of Ni film (2×10^{12} dyne/cm^2), ν is Poisson's ratio of 0.3 [38,42], and λ is the magnetostriction constant of Ni film (~24 ppm). Based on Eq. (1), the calculated effective *H*-field is

$$H_{\text{eff},[01\bar{1}]}=469\ \text{Oe} \quad (4)$$

Under a cyclic *E*-field of ±6.7 kV/cm, FMR spectra were obtained at the angles of 0° (i.e., in-plane direction), 45°, and 90° (i.e., out-of-plane direction) between *H*-field and heterostructure plane, which are shown in Fig. 4. The maximum shifts of FMR field (ΔH_{r}) are 410, 490, and 210 Oe at 0°, 45°, and 90° as shown in Figs. 4(a)–4(c), corresponding to mean ME coupling coefficients $\alpha = \Delta H_{\text{r}}/\Delta E$ of 102.5, 122.5, and 52.5 Oe·cm/kV, respectively. The complete spectra of FMR varying with *E*-field at the three angles are presented in Figs. S1–S3 in the Electronic Supplementary Material (ESM). It is worth mentioning that the observed value of 410 Oe is approximate to the calculated value of 469 Oe (Eq. (4)). In the test of *E*-field regulated FMR shift, we note that the in-plane ME coupling coefficient α = 102.5 Oe·cm/kV is higher than the previously reported maximum (94 Oe·cm/kV) at room temperature [27]. The shift of FMR caused by the *E*-field in the Ni film is due to the piezoelectric strain effect in the ferroelectric PMN–PT substrate.

Moreover, the relationship between FMR and *E*-field is also plotted in Figs. 4(d)–4(f). By comparing the three results, it can be found that the shift of FMR at 45° is significantly larger than those at the other two angles. That is because the *E*-field produces strain on PMN–PT, that is, it causes a large lattice strain at 45°, leading to a large magnetic anisotropy field at 45°, and further results in a large FMR shift in Ni film at 45°. Interestingly, the tunable FMR by *E*-field exhibits a characteristic butterfly shape, further revealing the converse ME coupling caused by strain/stress mechanism in Ni/PMN–PT multiferroic heterostructure. Meanwhile, the three butterfly-shaped curves appear two different variation trends, indicating that magnetic anisotropy exists in the Ni thin film, and these different variation trends maybe result from strain responses in different crystalline directions of the (011) cut PMN–PT substrate. At the above experimental stages, not only a large FMR shift of 490 Oe can be clearly observed, but also

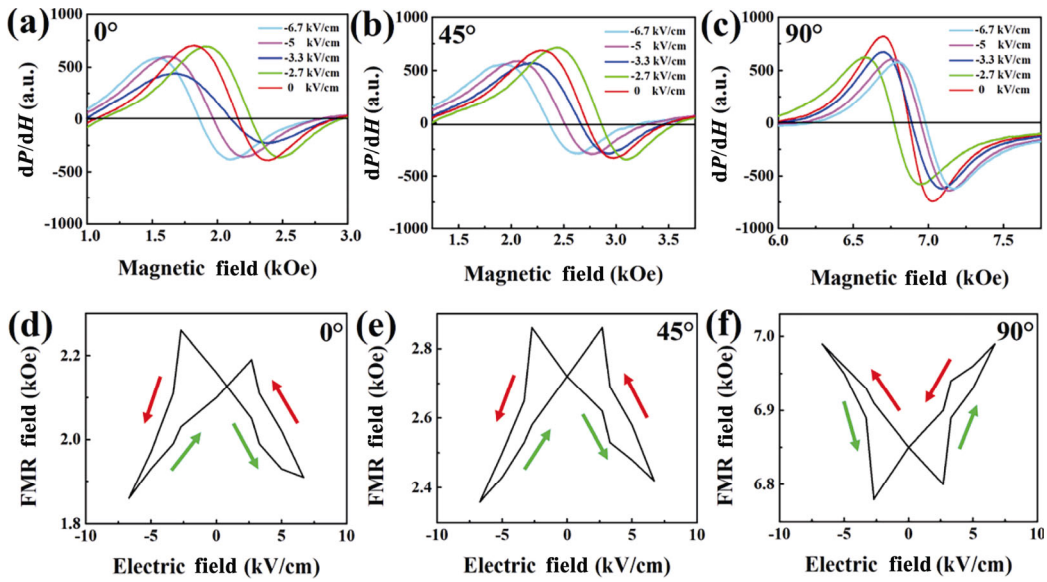

Fig. 4 *E*-field dependence of FMR at the angles of 0°, 45°, and 90° between *H*-field and heterostructure plane in Ni/PMN–PT multiferroic heterostructure.

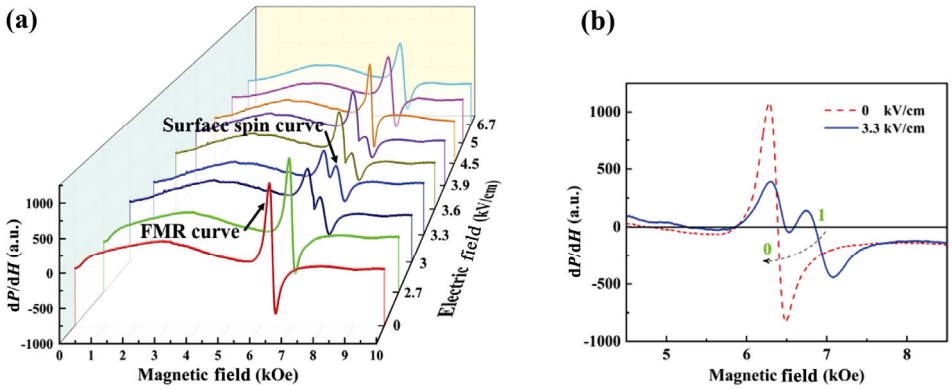

Fig. 5 (a) *E*-field dependence and (b) control of spin wave in Ni/PMN–PT multiferroic heterostructure at room temperature.

a reversible *E*-field tunability is shown completely in Ni/PMN–PT multiferroic heterostructure.

It is worth mentioning that both FMR and surface spin wave modes are observed under *E*-field (as shown in Fig. 5(a)) at the angle of 80° between *H*-field and heterostructure plane in Ni/PMN–PT heterostructure. Clearly, the strongest surface spin wave is excited by a small *E*-field of 3.3 kV/cm at room temperature, which has never been reported. This is probably owing to the unequal upper and lower interface conditions of the Ni layer, that is, one free surface and one faying surface with the PMN–PT. The relatively large lattice mismatch between Ni and PMN–PT causes larger lattice strain, which makes the exchange coupling interaction among spin in Ni/PMN–PT stronger than that in LSMO/PMN–PT multiferroic heterostructure, so that the surface spin wave can be excited by a smaller *E*-field of 3.3 kV/cm at room temperature. At this angle, *E*-field can regulate the surface spin waves "1" and "0" as shown in Fig. 5(b). Therefore, switching control can be realized in spin dynamics devices.

4 Conclusions

In summary, *E*-field-tuning non-volatile magnetic anisotropy and surface spin wave switch have been successfully certified in Ni/PMN–PT multiferroic heterostructures, wherein a conspicuous *E*-field regulated FMR shift of ca. 490 Oe arisen from strain/stress effect was observed, and the ME coupling coefficient α came to 122.5 Oe·cm/kV. Furthermore, at the angle of 80° between *H*-field and heterostructure plane, the surface spin wave mode can be switched to "1" or "0" via the applied *E*-field, particularly at room temperature, which might be enabled for *E*-field controllable logic device. The achievements of this study make the Ni/PMN–PT multiferroic heterostructures promising candidates for developing novel *E*-field tunable magnonics or spintronics devices.

Acknowledgements

This work was supported by the National Natural Science Foundation of China (Nos. 51772126, 21978110, and 52171210), Jilin Province Science and Technology Development Program (Nos. 20200201277JC, 20200201279JC, and 20200201187JC), and the Key Laboratory of Functional Materials Physics and Chemistry of the Ministry of Education (Nos. 2017002, 2016010, 2015003, and 2015011).

Electronic Supplementary Material

Supplementary material is available in the online version of this article at https://doi.org/10.1007/s40145-021-0548-0.

References

[1] Guo Q, Xu XG, Wang F, *et al*. In-plane electric field controlled ferromagnetism and anisotropic magnetoresistance in an LSMO/PMN–PT heterostructure. *Nanotechnology* 2018, **29**: 224003.

[2] Qin HJ, Dreyer R, Woltersdorf G, *et al*. Electric-field control of propagating spin waves by ferroelectric domain-wall motion in a multiferroic heterostructure. *Adv Mater* 2021, **33**: 2100646.

[3] Rana B, Otani Y. Towards magnonic devices based on voltage-controlled magnetic anisotropy. *Commun Phys* 2019, **2**: 90.

[4] Hu JM, Li Z, Wang J, *et al*. Electric-field control of strain-mediated magnetoelectric random access memory. *J Appl Phys* 2010, **107**: 093912.

[5] Zhao SS, Zhou ZY, Peng B, *et al*. Quantitative determination on ionic-liquid-gating control of interfacial magnetism. *Adv Mater* 2017, **29**: 1606478.
[6] Chen C, Barra A, Mal A, *et al*. Voltage induced mechanical/spin wave propagation over long distances. *Appl Phys Lett* 2017, **110**: 072401.
[7] Gómez JE, Vargas JM, Avilés-Félix L, *et al*. Magnetoelectric control of spin currents. *Appl Phys Lett* 2016, **108**: 242413.
[8] Zhao YL, Sun Y, Pan LQ, *et al*. Probing ferromagnetic/ferroelectric interfaces via spin wave resonance. *Appl Phys Lett* 2013, **102**: 042404.
[9] Neusser S, Grundler D. Magnonics: Spin waves on the nanoscale. *Adv Mater* 2009, **21**: 2927–2932.
[10] Hoffmann A, Bader SD. Opportunities at the frontiers of spintronics. *Phys Rev Appl* 2015, **4**: 047001.
[11] Liu HL, Zhang C, Malissa H, *et al*. Organic-based magnon spintronics. *Nat Mater* 2018, **17**: 308–312.
[12] Dumas RK, Åkerman J. Channelling spin waves. *Nat Nanotechnol* 2014, **9**: 503–504.
[13] Grundler D. Nanomagnonics around the corner. *Nat Nanotechnol* 2016, **11**: 407–408.
[14] Freitas VF, Dias GS, Protzek OA, *et al*. Structural phase relations in perovskite-structured $BiFeO_3$-based multiferroic compounds. *J Adv Ceram* 2013, **2**: 103–111.
[15] Liu WL, Liu M, Ma R, *et al*. Mechanical strain-tunable microwave magnetism in flexible $CuFe_2O_4$ epitaxial thin film for wearable sensors. *Adv Funct Mater* 2018, **28**: 1705928.
[16] Liu M, Howe BM, Grazulis L, *et al*. Voltage-impulse-induced non-volatile ferroelastic switching of ferromagnetic resonance for reconfigurable magnetoelectric microwave devices. *Adv Mater* 2013, **25**: 4886–4892.
[17] Figerez SP, Tadi KK, Sahoo KR, *et al*. Molybdenum disulfide-graphene van der Waals heterostructures as stable and sensitive electrochemical sensing platforms. *Tungsten* 2020, **2**: 411–422.
[18] Thiele C, Dörr K, Bilani O, *et al*. Influence of strain on the magnetization and magnetoelectric effect in $La_{0.7}A_{0.3}MnO_3$/PMN–PT(001) (A = Sr, Ca). *Phys Rev B* 2007, **75**: 054408.
[19] Molegraaf HJA, Hoffman J, Vaz CAF, *et al*. Magnetoelectric effects in complex oxides with competing ground states. *Adv Mater* 2009, **21**: 3470–3474.
[20] Zhang Y, Chen XY, Xie B, *et al*. Leakage current characteristics of $SrTiO_3$/$LaNiO_3$/$Ba_{0.67}Sr_{0.33}TiO_3$/$SrTiO_3$ heterostructure thin films. *Rare Met* 2021, **40**: 961–967.
[21] Liou YD, Chiu YY, Hart RT, *et al*. Deterministic optical control of room temperature multiferroicity in $BiFeO_3$ thin films. *Nat Mater* 2019, **18**: 580–587.
[22] Li CJ, Huang LS, Li T, *et al*. Ultrathin $BaTiO_3$-based ferroelectric tunnel junctions through interface engineering. *Nano Lett* 2015, **15**: 2568–2573.
[23] Garcia V, Bibes M, Bocher L, *et al*. Ferroelectric control of spin polarization. *Science* 2010, **327**: 1106–1110.
[24] Hu JM, Li Z, Chen LQ, *et al*. Design of a voltage-controlled magnetic random access memory based on anisotropic magnetoresistance in a single magnetic layer. *Adv Mater* 2012, **24**: 2869–2873.
[25] Oh N, Park S, Kim Y, *et al*. Magnetic properties of M-type strontium ferrites with different heat treatment conditions. *Rare Met* 2020, **39**: 84–88.
[26] Zhu MM, Nan TX, Peng B, *et al*. Advances in magnetics epitaxial multiferroic heterostructures and applications. *IEEE Trans Magn* 2017, **53**: 0800116.
[27] Xu H, Feng M, Liu M, *et al*. Strain-mediated converse magnetoelectric coupling in $La_{0.7}Sr_{0.3}MnO_3$/$Pb(Mg_{1/3}Nb_{2/3})O_3$–$PbTiO_3$ multiferroic heterostructures. *Cryst Growth Des* 2018, **18**: 5934–5939.
[28] Lou J, Liu M, Reed D, *et al*. Giant electric field tuning of magnetism in novel multiferroic FeGaB/lead zinc niobate–lead titanate (PZN–PT) heterostructures. *Adv Mater* 2009, **21**: 4711–4715.
[29] Behroozfar A, Hossain Bhuiyan ME, Daryadel S, *et al*. Additive printing of pure nanocrystalline nickel thin films using room environment electroplating. *Nanotechnology* 2020, **31**: 055301.
[30] Luo JK, Flewitt AJ, Spearing SM, *et al*. Young's modulus of electroplated Ni thin film for MEMS applications. *Mater Lett* 2004, **58**: 2306–2309.
[31] Zhao SF, Zeng LZ, Cheng G, *et al*. Ni/Co-based metal-organic frameworks as electrode material for high performance supercapacitors. *Chin Chem Lett* 2019, **30**: 605–609.
[32] Luo JK, Pritschow M, Flewitt AJ, *et al*. Effects of process conditions on properties of electroplated Ni thin films for microsystem applications. *J Electrochem Soc* 2006, **153**: D155.
[33] Gilbert I, Chavez AC, Pierce DT, *et al*. Magnetic microscopy and simulation of strain-mediated control of magnetization in PMN–PT/Ni nanostructures. *Appl Phys Lett* 2016, **109**: 162404.
[34] Bai H, Li J, Hong Y, *et al*. Enhanced ferroelectricity and magnetism of quenched $(1-x)BiFeO_3$–$xBaTiO_3$ ceramics. *J Adv Ceram* 2020, **9**: 511–516.
[35] Han PD, Yan WL, Tian J, *et al*. Cut directions for the optimization of piezoelectric coefficients of lead magnesium niobate–lead titanate ferroelectric crystals. *Appl Phys Lett* 2005, **86**: 052902.
[36] Zheng LM, Jing YJ, Lu XY, *et al*. Temperature and electric-field induced phase transitions, and full tensor properties of $[011]_C$-poled domain-engineered tetragonal $0.63Pb(Mg_{1/3}Nb_{2/3})$–$0.37PbTiO_3$ single crystals. *Phys Rev B* 2016, **93**: 094104.
[37] Wu T, Zhao P, Bao MQ, *et al*. Domain engineered switchable strain states in ferroelectric (011) $[Pb(Mg_{1/3}Nb_{2/3})O_3]_{(1-x)}$–$[PbTiO_3]_x$ (PMN–PT, $x \approx 0.32$) single crystals. *J Appl Phys* 2011, **109**: 124101.
[38] Liu M, Obi O, Cai ZH, *et al*. Electrical tuning of magnetism in Fe_3O_4/PZN–PT multiferroic heterostructures

derived by reactive magnetron sputtering. *J Appl Phys* 2010, **107**: 073916.

[39] Jung J, Lee W, Kang W, *et al*. Review of piezoelectric micromachined ultrasonic transducers and their applications. *J Micromech Microeng* 2017, **27**: 113001.

[40] Ye FJ, Dai HY, Peng K, *et al*. Effect of Mn doping on the microstructure and magnetic properties of $CuFeO_2$ ceramics. *J Adv Ceram* 2020, **9**: 444–453.

[41] Zhu MM, Zhou ZY, Peng B, *et al*. Modulation of spin dynamics via voltage control of spin-lattice coupling in multiferroics. *Adv Funct Mater* 2017, **27**: 1605598.

[42] Politano A, Chiarello G. Probing the Young's modulus and Poisson's ratio in graphene/metal interfaces and graphite: A comparative study. *Nano Res* 2015, **8**: 1847–1856.